International Journal of Engineering Science Invention
ISSN (Online): 2319 – 6734, ISSN (Print): 2319 – 6726
www.ijesi.org ||Volume 6 Issue 3|| March 2017 || PP. 54-65

Numerical Simulation of Flow in a Solid Rocket Motor: Combustion Coupled Pressure Dependent Regressive Boundary

Mehmet Ozer Havlucu[1], Kadir Kirkkopru[2]
[1](*Department of Mechanical Engineering/Istanbul Technical University, Istanbul, Turkey)*
[2](*Department of Mechanical Engineering/Istanbul Technical University, Istanbul, Turkey)*

ABSTRACT*: Acomputational study is performed for the simulation of reactive fluid flow in a solid rocket motor chamber with pressure dependent propellant burning surface regression. The model geometry consists of a 2D end burning lab-scale motor. Complete conservation equations of mass, momentum, energy and species are solved with finite rate chemistry. The pressure dependent regressive boundary in the combustion chamber is treated by use of remeshing techniques. Hydrogen and propane combustion processes are examined. Time dependent pressure and burning rate variations are illustrated comprehensively. Temperature and species mass fraction variations are given within the flame zone. Temperature, velocity and density distributions are compared for both constant burning rate and pressure dependent burning rate simulations.*

KEYWORDS -*Combustion, Regression, Remeshing, Solid Rocket Motor*

I. INTRODUCTION

Solid rocket motors (SRMs) are devices which convert chemical-thermal energy into kinetic energy. Solid propellant burns through chemical reactions into hot gas mixture inside the combustion chamber in SRM. Ejection of these hot gases from the nozzle with high speed produces thrust and thus propels the rocket forward. For this reason, the control of SRM requires thorough understanding of combustion coupled gas flow associated with regressing solid fuel boundary, which is an extremely complicated phenomenon [1].

Studies on this topic started nearly half a century ago. Early workers studied the gas flow in chamber with cold-flow approach where inert gases are injected into the chamber. Velocity distributions were obtained analytically for incompressible laminar flow [2, 3]. Dunlap et al [4] performed experiments on cold flow field that develops along a cylindrical part of rocket chamber and studied injection driven flow with injection Mach numbers 0.0018 and 0.0036 to achieve centerline Mach numbers of 0.14 and 0.27, respectively. Accordingly, Traineau et al. [5] conducted cold flow simulation tests of a nozzleless solid rocket motor using a 2-D duct and examined pressure and Mach number variations along this motor. Thereafter, the compressibility effect is illustrated analytically by Balakrishnan et al.[6].

The reaction zone is very thin in solid rocket motors, in the order of few millimeters and complicated to be described mathematically [7]. Modeling of this thin layer requires challenging computational effort. For this reason, researchers are initially encouraged to model the flow in the chamber as cold flow induced by mass inflow from porous side walls mimicking the propellant surface. For example, 2D simulations were studied on a simple cylindrical motor with models representing propellant combustion response by Vuillot et al. [8]. Euler and Navier-Stokes equations were examined in a 2D test case representing SRM using artificial viscosity terms by Lupoglazoff and Vuillot [9]. Kirkkopru and his co-workers solved Navier-Stokes equations numerically in an axisymmetric cylindrical solid rocket motor chamber with sidewall injection to study the generation of vorticity by periodic pressure disturbance at the exit [10]. Zhao et al. [11] studied on a mathematical model which describes the evolution of unsteady vorticity by low Mach number sidewall mass addition in a cylinder. Using a Navier-Stokes solver, an efficient conductive heat transfer model by combining gas flow and heat transfer to the propellant was developed by Alavilli and his co-workers [12].

The design and the performance of SRMs depend heavily on combustion processes and fluid flow, since trust in SRMs is generated through chemical reaction and expansion and acceleration of chemical products by passage through a nozzle at the rear of the rocket. Therefore, reactive fluid flow and understanding its characteristics are the important aspects of SRMs. As computational powers increased, researchers started to combine the cold flow with reaction to reveal the characteristics of reactive fluid flow. Numerical analysis of combustion dynamics of SRM with stagnant wall boundaries was studied by Apte and Yang [13]. El-Askary and his co-workers described combustion process in a SRM combustion chamber considering 2D, multi component

reactants with turbulent compressible flow [14]. Chu et al. [15], studied unsteady state response of a laminar flame to acoustic waves in a two dimensional combustion chamber with surface mass injection. Yumusak [16] developed a computational method to perform internal flow of two dimensional system using Euler equations.

The solid rocket motor propellant is the fundamental propulsion concept for both tactical and strategically missiles. Solid propellant is a heterogeneous mixture of an oxidizer, a binder and a metallic powder as a fuel and other additives. An example for the oxidizer is ammonium perchlorate (AP) and for the binder is cured hydroxyl terminated polybutadiene (HTPB). The ballistic behavior of the solid propellant is affected by the burning rate. As combustion takes place, combustion chamber geometry is no longer constant due to the regression of the solid fuel as it turns into the gaseous mixture. Burning area changes result in changes in flow field inside the chamber of rocket motors. Thus, the burning rate of propellants plays a significant role in controlling the parameters such as thrust of rocket motors; therefore it is important to model the burning rate in solid rocket motor simulations. [17]. In order to serve this, Uygun and Kirkkopru [18] simulated the flow in SRM chamber considering two-dimensional unsteady cold flow with regressing propellant boundary. Terzic and his co-workers [19] conducted numerical simulation of pressure dependent burning surface regression without chemical reactions to predict internal ballistics performance of solid propellant rocket motors.

Different definitions are given for the burning rate in the literature [7,20-24]. For example, it is defined as the regression rate of the solid propellant in parallel layers and perpendicular to the propellant surface [19,25]. In some studies, it is defined as the distance travelled by the flame front per unit time perpendicular to the propellant surface [26]. The pressure of the combustion chamber, the initial temperature of the solid propellant, the composition of the propellant and the particle size of the oxidizer [7,19,22-25] are the main parameters which affect the burning rate.

Since the other key factor contributing to the SRMs design and performance is regressive burning surface [20], in the present work, a computational method is developed to simulate chemical reaction coupled with gas flow inside the combustion chamber of SRM with pressure dependent regressive boundary. The model was applied to compressible two-dimensional channel flow in a lab-scale motor. Finite volume discretization is utilized and Euler equations with finite rate chemistry are solved with mass, energy and species equations. This reactive gas flow model with constant burning rate was validated against the study by Yumusak [16] in the earlier study of the authors [27].

Initially, the configuration of the SRM model where the chemical combustion process with gas flow takes places is described in this study. Then, the mathematical model and governing equations of the reacting flow under considered geometry is illustrated comprehensively. Boundary conditions, chemical and numerical models are explained. Pressure dependent burning rate with regressing boundary model combined with reacting flow in a combustion channel is performed. Time dependent burning rate and pressure changes are described. Temperature and species distribution within the flame zone are given at time when all the solid fuel is consumed. H_2 and C_3H_8 based combustion reactions are studied. Temperature, velocity and density variations of the gas mixture are examined and compared both for constant burning rate and pressure dependent burning rate simulations.

II. COMPUTATIONAL (GEOMETRICAL) MODEL

Fig. 1 represents a schematic combustion chamber of SRM with 2-D end-burning lab-scale motor. The chamber length is 170 mm. The half-height of the chamber is 45 mm. The combustion chamber is connected to a converging-diverging nozzle with a half throat height of 16.77 mm and radius of curvature of 30 mm. Overall chamber length including the nozzle is 270 mm. The attached solid fuel is 100 mm thick.

The upper part is symmetric boundary. Lower one is an impermeable wall. The gaseous fuel premixed with O_2 is injected at low Mach number subsonic conditions from the head-end surface perpendicular to the main stream. On this boundary, solid propellant surface degrades, as it burns. The computational model for pressure dependent boundary regression to the left is explained in Section 7. The gaseous mixture leaves the combustion chamber through the nozzle at supersonic conditions.

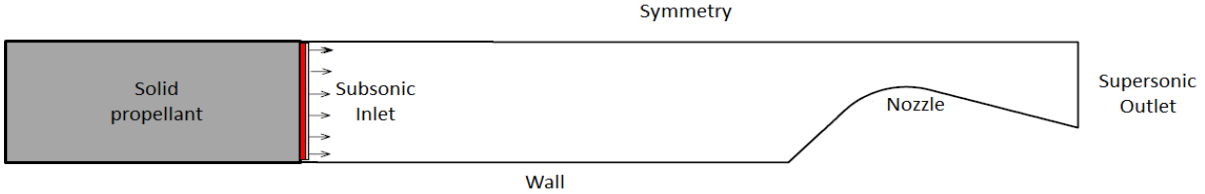

Figure 1. Geometric representation of the lab-scale motor [14]

III. GOVERNING EQUAT ONS

The two-dimensional compressible reactive flow model used in this study is based on conservation equations of mass, momentum, energy, and species concentrations for all multicomponents of the chemically reacting system. For a system with N number of species, the governing equations of time dependent Euler equations take the following generic vector form.

$$\frac{\partial Q}{\partial t} + \frac{\partial F}{\partial x} + \frac{\partial G}{\partial y} = H$$

Where*Q*, *F*, *G* and *H* are

$$Q = \begin{bmatrix} \rho \\ \rho u \\ \rho v \\ \rho E \\ \rho Y_1 \\ \rho Y_2 \\ \cdots\cdots \\ \cdots\cdots \\ \rho Y_{N-1} \end{bmatrix} \qquad F = \begin{bmatrix} \rho u \\ \rho u^2 + p \\ \rho uv \\ [\rho E + p]u - \rho \sum_{i=1}^{N} h_i D_i \frac{\partial Y_i}{\partial x} - k \frac{\partial T}{\partial x} \\ \rho Y_1 u - \rho D_1 \frac{\partial Y_1}{\partial x} \\ \rho Y_2 u - \rho D_2 \frac{\partial Y_2}{\partial x} \\ \cdots\cdots\cdots \\ \cdots\cdots\cdots \\ \rho Y_{N-1} u - \rho D_{N-1} \frac{\partial Y_{N-1}}{\partial x} \end{bmatrix}$$

and

$$G = \begin{bmatrix} \rho v \\ \rho uv \\ \rho v^2 + p \\ [\rho E + p]v - \rho \sum_{i=1}^{N} h_i D_i \frac{\partial Y_i}{\partial y} - k \frac{\partial T}{\partial y} \\ \rho Y_1 v - \rho D_1 \frac{\partial Y_1}{\partial y} \\ \rho Y_2 v - \rho D_2 \frac{\partial Y_2}{\partial y} \\ \cdots\cdots\cdots \\ \cdots\cdots\cdots \\ \rho Y_{N-1} v - \rho D_{N-1} \frac{\partial Y_{N-1}}{\partial y} \end{bmatrix} \qquad H = \begin{bmatrix} 0 \\ 0 \\ 0 \\ q \\ s_1 \\ s_2 \\ \cdots \\ \cdots \\ s_{N-1} \end{bmatrix}$$

Here,ρ, u, v, p, E, and Y_N represent the total density, x velocity, y velocity, pressure, the total energy and the mass fraction of the Nth species, respectively. $h_i$is the mass enthalpy for the i^{th} species, $D_i$is the diffusion coefficient and $q$is the heat of the chemical reaction. Source term,S_N, includes contributions from chemical reactions taking place inside the combustion chamber and it represents the rate of change of every species due to the chemical reaction.

The thermodynamic properties are assumed to be thermally perfect. The specific heat of the species is taken as a function of temperature and perfect gas mixing law is used for the mixture specific heat within the domain. The flow is assumed to be laminar everywhere in the domain. Gravitational force and radiative heat transfer are neglected.

IV. BOUNDARY CONDITIONS

There are four boundary conditions representing the lab-scale model. The left side of the model which is the end-burning part is taken as a subsonic inlet. The mass flux at this injecting boundary is calculated with respect to solid fuel regression rate as will be explained in Section 7. The injection temperature is 350 K as in the study by Havlucu and Kirkkopru [27]. The fuel-air equivalence ratio is taken 0.7. The upper side has a symmetry boundary condition. The lower solid impermeable boundary and the nozzle wall are adiabatic. The gaseous mixture leaves the nozzle at supersonic conditions. For supersonic outflow the flow properties are calculated from the interior points.

V. CHEMICAL MODEL

Despite the recent developments in computational power, thorough consideration of all physical and chemical processes in SRM and modeling of those are still challenging. Therefore, researchers are encouraged to use simplified reaction mechanisms to describe the combustion process [13,14,16]. In this study, firstly combustion of hydrogen gas is considered. This combustion process is assumed to follow a two-step model, where in the first step hydrogen reacts with oxygen to form hydroxide and in the second step hydroxide combines with hydrogen to compose gaseous water molecule. This reaction mechanism has been well established and captures information about the major chemical kinetic pathways. It can be represented by the following steps [28].

$$H_2 + O_2 \leftrightarrow 2OH$$
$$2OH + H_2 \leftrightarrow 2H_2O$$

The second combustion model which is studied in the present work is propane combustion. The combustion of propane is assumed to follow a one-step reaction, which yields carbon dioxide and water vapor as products.

$$C_3H_8 + 5O_2 \rightarrow 3CO_2 + 4H_2O$$

VI. NUMERICAL MODEL

The commercial software ANSYS Fluent 15.0 [29] is used to solve the governing equations coupled with the chemical reactions. The combustion process is modeled using finite rate chemistry. Spatial discretization is achieved using second order upwind differencing scheme and first order implicit method is used for temporal discretization.

Temperature and species mass fractions vary very rapidly within a very thin zone adjacent to the boundary mimicking the propellant surface. Thus, to better capture these rapid variations of flow properties within this thin regime, cells are highly clustered in the neighborhood of the end burning part of the motor as were done by others [12,13,15,18]. Fig. 2 shows the computational grids near the head-end of the computational domain. The smallest cell which is next to the transpiring left-hand wall is taken as 0.015 mm thick. The dimensions of the subsequent ones in axial direction are set to be 1.05 times the previous one. This sizing strategy in gridding holds till 30 mm away from the head end boundary. Beyond this place onwards, the sizes of the grids are taken uniform. 50 uniform and 224 non-uniform grids are used in the vertical and horizontal directions, respectively. Under-relaxation factor of 0.65 within each time step is used for pressure, momentum and temperature for numerical stability.

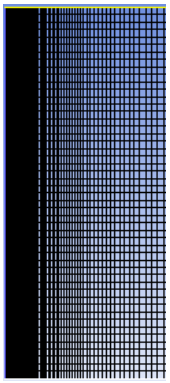

Figure 2. Grid structure next to the end-burning boundary

The convergence residuals for continuity, velocity, energy, and mass fractions of the species are set to be $10^{-3}$for every iteration in each time step for time dependent calculations. When the steady state results are reached, the absolute residual of energy and velocity are $5x10^{-5}$ and $7x10^{-5}$, respectively.

Steady state solution is obtained firstly as an initial condition for the unsteady pressure dependent regressive head-end boundary condition. Steady state solution is achieved by setting the temperature at all grid points equal to the adiabatic flame temperature of the combustion model. Accordingly, the velocity field and species mass fractions in the domain are taken equal to the inlet velocity and species mass fractions at the end burning boundary. Non-regressive steady chemical reaction model was verified against the Euler type study of Yumuşak [16] in our previous work [27], when constant regression rate model was introduced.

VII. PRESSURE DEPENDENT REGRESSIVE BOUNDARY MODEL

SRM has a variable internal geometry due to the transformation of the solid propellant to form combustion products. This variation in geometry is called surface regression. Changing combustion volume in time results in change of pressure and thrust and thus causing a change in SRM performance.

Here, surface regression is modeled with a layer between solid propellant grain and the gases which are the fuel-air mixture as shown in Fig. 3 as in the study of [30]. The left part is solid fuel with oxidizer. The red zone is the layer where solid fuel is vaporized to form reactant and oxidizer gases. Therefore, it is assumed that the reaction starts at the interface between the red zone and the chamber. As combustion occurs, the amount of the solid fuel decreases and the boundary regresses to the left. Displacement of the burning surface is considered as parallel layers normal to burning surface of the propellant grain [19,27]. The movement of this boundary is governed by the chamber pressure dependent burning rate $\dot{r}_b$.

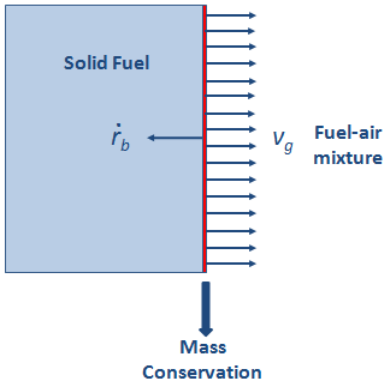

Figure 3. Surface Regression Model [30]

As surface regresses with burning rate $\dot{r}_b$, the reactant and oxidizer gases leave the burning surface in opposite direction with the velocity V_g. Since the propellant density ρ_p is much higher than the density of the gaseous reactant and oxidizer mixture ρ_g, the velocity of this mixture is significantly greater than the burning rate. Thus, conservation of mass is approximately [30]:

$$\rho_p \dot{r}_b \approx \rho_g V_g \quad (1)$$

Here, the velocity V_g or the mass flux $\rho_g V_g$ can be determined through equation 1, because the density of the propellant is known and the burning rate can be calculated using the below equation 2.

In the literature, some formulations are offered to predict the burning rate of an energetic solid propellant [7,19,22-25]. One of the well-known formulations is the APN model, which approximates the burning rate as solely dependent on the mean local pressure within the combustion chamber [19].

In the current study, the burning rate of the solid propellant is simulated using the APN model as follows;

$$\dot{r_b} = \alpha p^n \quad (2)$$

This is known as Saint Robert's law or Vieille's law [30,31]. In this equation, $\dot{r_b}$ is the pressure dependent burning rate.$\alpha$is a constant which depends on the initial temperature of the solid propellant. It has a value between 0.002 and 0.05. *p* is the chamber pressure. $n$is the pressure index which strongly depends on the type of the propellant. For double base propellants n has a value between 0.2 and 0.6. For ammonium perchlorate it takes the value between 0.1 and 0.4. The values of α and n cannot be predicted theoretically. They are determined experimentally. For a particular propellant, minimum of five tests using propellant strands at constant pressure is used for determining the values of α and n. These tests should be performed at minimum three different pressures. [26]

To numerically model the regression of the burning surface boundary, user-defined functions (UDF) are customized using C++ [32] and implemented in ANSYS Fluent 15.0 [29]. Displacement of the boundary is considered only perpendicular to the boundary surface. With this assumption, the end burning boundary regression is calculated using the below expression:

$$x_{new} = x_{old} - \dot{r}_b \Delta t$$

Here, x_{new} is the calculated new x-coordinate of the boundary at the end of the time step Δt. xold is the x-coordinate of the boundary in the previous time step.$\dot{r}_b$is the burning rate.

For the constant burning rate simulations, a UDF "DEFINE_GRID_MOTION" is used to move the regressive burning solid propellant boundary as in the work of Havlucu and Kirkkopru [27]. It is customized in C++ so that at the end of every time step, the new location of the moving boundary is calculated using the above equation and then updated by use of the UDF. During the unsteady combustion process with regressive boundary new vertical uniform grid lines are added in the horizontal direction. This method is named as Dynamic Layering Method in ANSYS Fluent 15.0. It allows specifying a desired layer height next to the moving boundary. There are two options for the layering method which are constant height and constant ratio procedure. In the current study, constant height for cell spacing is performed.

For the pressure dependent burning rate simulations, the following UDF's are added to the solver. These are "DEFINE_EXECUTE_AT_END" and "DEFINE_PROFILE". At the end of the every time step, the UDF "DEFINE_EXECUTE_AT_END" is called in order to calculate the average pressure in the combustion chamber. Using the pressure dependent burning rate expression which is proposed by Vieille, the burning rate of the solid fuel is calculated. Since the density of the propellant is known, the inlet gas mixture velocity on the burning boundary is calculated as illustrated before. Then the "DEFINE_PROFILE" UDF is called in order to update the velocity inlet at the solid fuel boundary. Finally the "DEFINE_GRID_MOTION" is performed to move the regressing boundary according to the calculated burning rate within the time step. After all of these calculations have been done, the solver continues to the next time step. This procedure is done until all the solid fuel is consumed.

At the end of every time step, new rectangular grids are added to the left of the computational domain for every regression distance of 0.03 mm using Dynamic Layering Method offered by ANSYS Fluent 15.0. The initial thickness of the propellant 100 mm is added to the total length of 270 mm. Depending on the burning rate, the propellant is consumed between the 11^{th} and 14^{th} seconds.

For the calculations with regressive propellant, time dependent equations for non-regressive boundary model with chemical reaction are solved until steady state is reached for the given inlet temperature. Then, these steady results are set as initial conditions for the unsteady simulation of pressure dependent burning rate with regressive boundary, as done by others [18,27]. $\alpha$is taken as 0.01 for all the pressure dependent unsteady calculations regarding previous works [30,31]. Different pressure indexes n are used to investigate its effect on burning rate and chamber pressure. Fig. 4 compares the time dependent burning rates for n=0.2, 0.4 and 0.6 and constant burning rate. For n=0.2 the initial burning rate is the highest among the others, thus the solid fuel is consumed in a shorter time compared to n=0.4 and 0.6. For the three cases of n=0.2, 0.4 and 0.6 the solid fuel consumption times are 11.19 s, 12.53 s and 14 s, respectively. As combustion process continues the burning rates for all cases decrease in time, since the chamber pressure decreases, as the chamber volume increases.

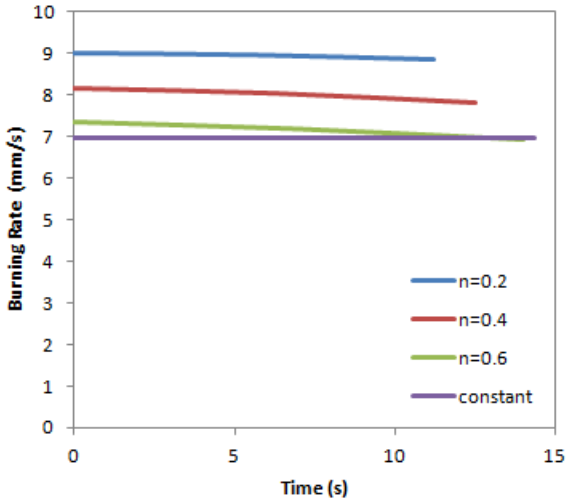

Figure 4. Comparison of Burning Rates for n values of 0.2, 0.4 and 0.6, where α=0.01 and for constant burning rate

In Fig. 5, the chamber pressure change in time is shown both for constant burning rate and pressure dependent burning rate for n values of 0.2, 0.4 and 0.6. The initial pressure is 0.6 MPa for all the simulations, a result from non-regressive steady state calculation. The pressure decreases 5% in the constant burning rate process due to the volume increase in geometry increase. However, the pressure decreases about 10% in the pressure dependent burning rate simulations. Because the burning rate depends on decreasing pressure leading to decreasing inlet mass velocity, this cycle induces faster pressure decrement in time compared to that for constant burning rate.

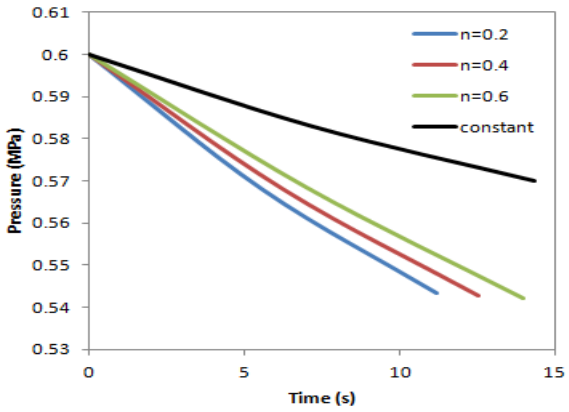

Figure 5. Variation of Chamber Pressure with time for n values of 0.2, 0.4 and 0.6, where α=0.01 and for constant burning rate

Within the very thin flame zone close to solid propellant surface, the spatial variations of temperature and species mass fractions are very rapid as depicted in Fig. 6. The temperature increases from the feeding boundary

temperature 350 K to 1902 K in a two millimeter distance. The flow characteristics within this region are captured using grids that are highly clustered near the head-end burning part of the motor. Fig. 6 also compares mass fractions of H_2, O_2 and H_2O species along the axis of the combustion chamber. H_2 and O_2 mass fractions decrease from 0.0183 and 0.21 to 0 and 0.0636, respectively. The mass fraction of the product, H_2O, increases from 0 to 0.1647.

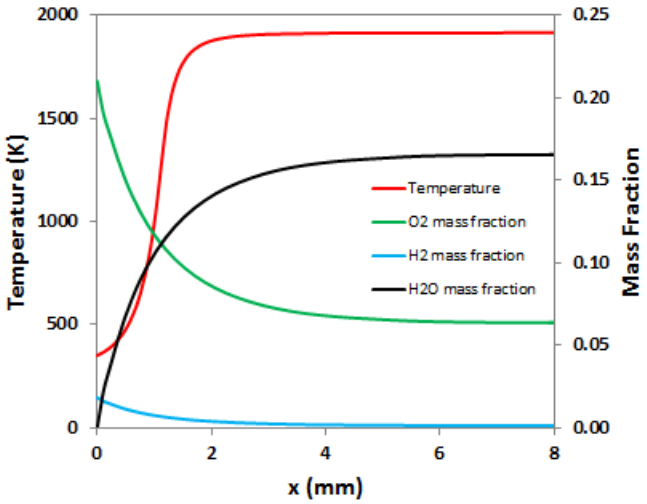

Figure 6. Spatial Variations of temperature and mass fractions along x-axis from the burning end with pressure

dependent burning rate when all the solid fuel is consumed at t=14 s. Here, $\mathbf{n}$=0.6 and $\boldsymbol{\alpha}$=0.01

Grid independency study is performed using various grid sizes. Fig. 7 shows the temperature profiles both for constant burning rate and pressure dependent burning rate for minimum grid sizes of 0.03 mm, 0.015 mm and 0.0075 mm with inlet temperature of 350 K at the time when all the solid fuel is consumed. It is observed that, considered grid sizes result in the same temperature profiles for both burning rate models. Thus for computational cost, minimum grid size of 0.03 mm is used in the present study.

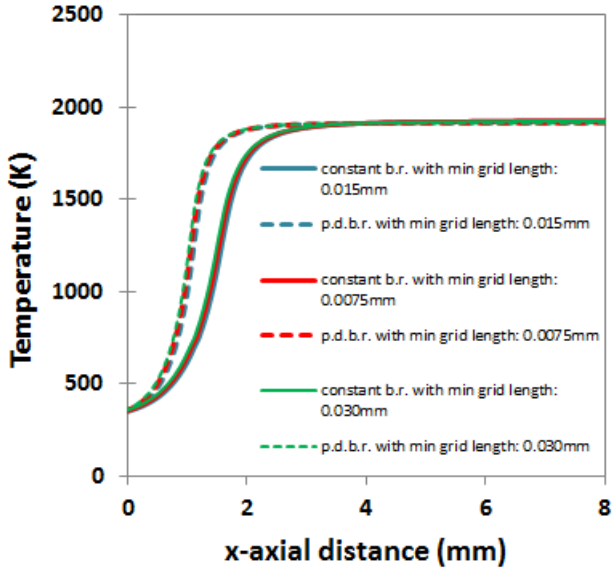

Figure 7. Temperature profiles from the burning end at the time when all the solid fuel is consumed with constant burning rate at t=14.35 s and pressure dependent burning rate at t=14 s, n=0.6 and α=0.01 for minimum grid sizes of 0.03 mm, 0.015 mm and 0.0075 mm when inlet temperature is 350 K

Fig. 8 illustrates temperature profiles for both constant and pressure dependent burning rate regression of the solid fuel boundary with an inlet temperature of 350 K. Considering an equivalence ratio of 0.7 for H_2 combustion, the temperature reaches a maximum value of 1918 K in constant burning rate and 1902 K in pressure dependent burning rate indicating that the maximum temperature is affected slightly by the pressure dependency of burning rate.

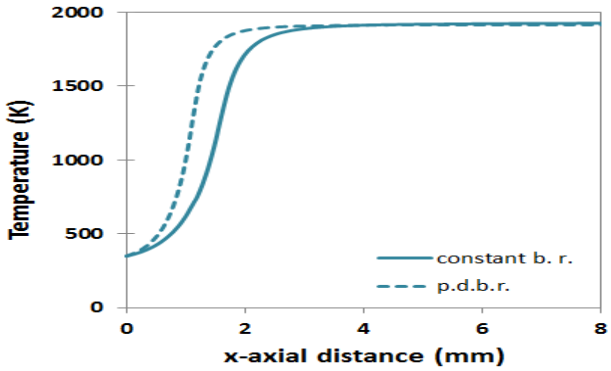

Figure 8. Temperature profiles from the burning end when all the solid fuel is consumed with constant burning rate at t=14.35 s and pressure dependent burning rate at t=14 s when n=0.6 and α=0.01, at inlet temperature of 350 K

Spatial temperature profiles for inlet temperatures of 350 K and 800 K for H_2 combustion were shown in Fig. 9. Temperature profile for inlet temperature of 800 K has a steeper spatial gradient than that for inlet temperature of 350 K, leading to a higher maximum gas mixture temperature of 2001 K compared to 1902 K for inlet temperature of 350 K.

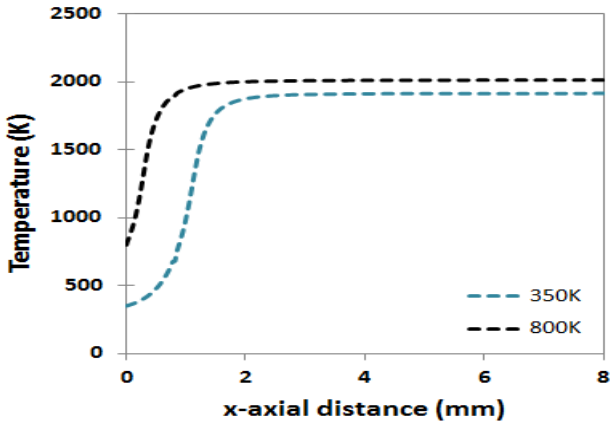

Figure 9. Temperature profiles from the burning end with pressure dependent burning rate when all the solid fuel is consumed corresponding t=14 s and n=0.6, α=0.01, inlet temperatures of 350 K and 800 K

Spatial temperature variations for H_2 and C_3H_8 in the chamber for the inlet temperature of 350 K are compared in Fig. 10. In the reaction zone, the temperature increases to 1902 K for the hydrogen combustion and to 1775 K for the propane combustion, respectively. These values were 1918 K and 1792 K for constant burning rate in the study of Havlucu and Kirkkopru [27], respectively. For both constant and pressure dependent burning rate the maximum temperature is achieved in the H_2 combustion, for the parameters under consideration.

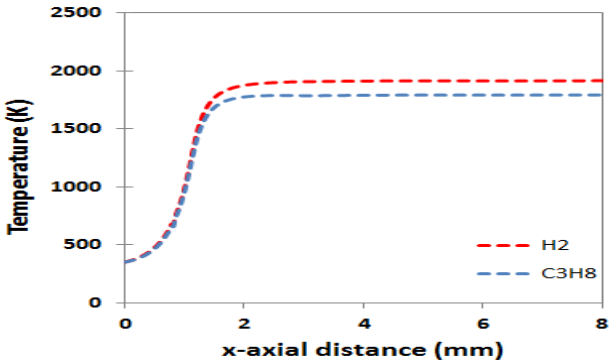

Figure 10. Temperature profiles from the burning end with pressure dependent burning rate when all the solid fuel is consumed at t=14 s, n=0.6 and α=0.01 for H_2 and C_3H_8 combustion

The axial velocity distribution along the x-axis corresponding to inlet temperature of 350 K for both constant rate regression and pressure dependent regression is presented in Fig. 11. The temperature of the gas mixture rises rapidly in the 2 mm thin reaction zone as shown in the previous figures. In this region, the mixture of combustion gases expands and the velocity of the gaseous mixture increases from 13.39 m/s to 74.26 m/s in the pressure dependent burning rate simulation and from 14.23 m/s to 77.76 m/s in the constant burning rate model in the study of Havlucu and Kirkkopru [26]. The flow inlet Mach number is 0.0363 and the flow Mach number reaches the value of 0.0859 at the end of the reactive flame zone for the pressure dependent regression model, which is slightly lower than the value obtained in the unsteady burning rate calculations [26]. This is due to decreasing pressure dependent burning rate with decreasing pressure in the chamber with increasing chamber volume.

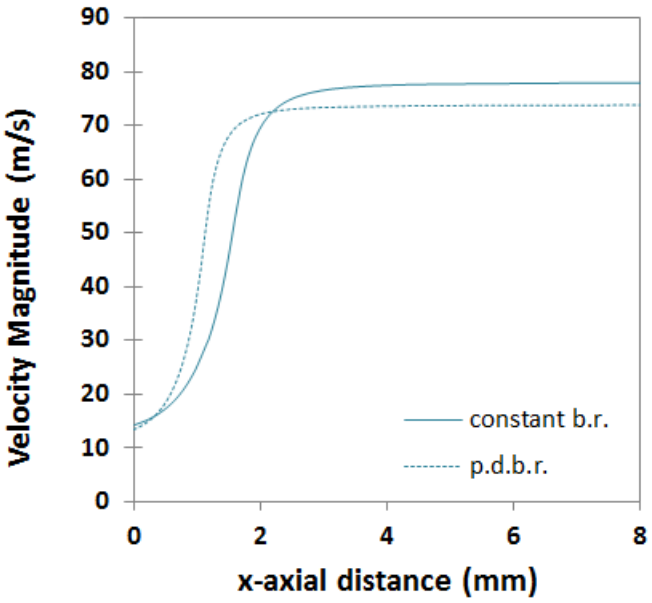

Figure 11. Axial variation of velocity of gas mixture from the burning end when all the solid fuel is consumed at t=14.35 s for constant burning rate and t=14 s, n=0.6 and α=0.01 for pressure dependent burning rate at inlet temperature of 350 K

Fig. 12 illustrates the density variation of the gas mixture both for constant and pressure dependent simulations when all the solid fuel is consumed. The density decreases from 0.85 kg/m^3 to 0.153 kg/m^3 for the pressure dependent model and from 0.8 kg/m^3 to 0.153 kg/m^3 for the constant burning rate model, respectively.

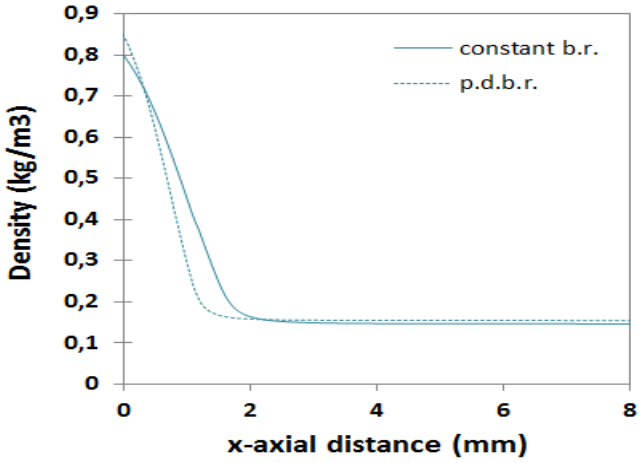

Figure 12. Density variation of gas mixture with distance from the burning end when all the solid fuel is consumed at t=14.35 s for constant burning rate and t=14 s, n=0.6 and α=0.01 for pressure dependent burning rate at inlet temperature of 350 K

VIII. CONCLUSION

In this work, the interaction between flow characteristics and combustion dynamics in a solid rocket motor chamber with pressure dependent burning rate on the head end burning boundary of a 2-D lab-scale motor was investigated computationally. Complete time dependent conservation equations for reacting flow were solved with finite rate chemistry. The pressure dependent regressive end-burning boundary in the chamber is treated by use of remeshing technique. Hydrogen and propane combustion models are used to represent the chemical model. The constant which depends on the initial solid fuel temperature, is a taken as 0.01 in all the calculations. The pressure index is taken 0.2, 0.4 and 0.6.

Results of the coupled simulation of the reactive fluid flow with propellant burning surface regression demonstrate that about 44 % of the chamber volume increase causes about 10 % decrease in chamber pressure in the pressure dependent burning rate simulation for the three different n values, whereas it was only 5 % in the constant burning rate one. In addition to that, burning rate decreases slightly in time as the burning boundary degrades. The thickness of the flame zone is decreased in pressure dependent burning rate model compared to that of constant burning rate due to the decreased inlet velocity. Therefore, the velocity and density high gradient zones are shrinked as well. Furthermore, the inlet temperature effect is investigated for hydrogen combustion. As the inlet temperature is increased, the maximum temperature is increased and the temperature profile becomes stiffer. Comparing the hydrogen and propane chemical models, hydrogen combustion model results in higher maximum temperature than that for propane for the same inlet conditions, a similar result to that in the constant burning rate simulation [27].

REFERENCES

[1] M. A. Willcox, M. Q. Brewster, K. C. Tang, D. S. Stewart and I. Kuznetsov, Solid Rocket Motor Internal Ballistics Simulation Using Three-DimensionalGrainBurnback, *J. Propul. Power, Vol. 23 (3)*, 2007, 575–584.

[2] G. I. Taylor,, Fluid Flow Regions Bounded by Porous Surfaces, *Proceedings of the Royal Society of London, Series 234A, Vol. 1199*,1956, 456-475.

[3] F. E. C. Culick, RotationalAxisymmetricMean Flow and Damping of Acoustic Waves in a Solid Propellant Rocket, *AIAA Journal, Vol. 4*, 1966, 1462-1464.

[4] R. Dunlap, A. M. Blackner, R. C. Waugh, R. S. Brown, and P. G. Willoughby, Internal Flow Field Studies in a Simulated Cylindrical Port Rocket Chamber, *J. Propul. Power, Vol. 6*, 1990, 690-704.

[5] J. C. Traineau, P.Hervat, and P. Kuentzmann, Cold-FlowSimulation of a Two-DimensionalNozzleless SolidRocket Motor, *AIAA Paper, 86-1447*, 1986.

[6] G. Balakrishnan, A.Linan, and F. A. Williams, RotationalInviscidFlow in Laterally Burning Solid-Propellant Rocket Motors, *Journal of Propulsion .and Power, Vol. 8*, 1992, 1167–1176.

[7] A.M. Hegab, H.H. Sait, A. Hussain, A.S,Said, 2014, Numerical Modeling for the Combustion of Simulated Solid Rocket Motor Propellant, *Computers & Fluids, Vol. 89*, 2014, 29-37.

[8] F. Vuillot, T. Basset, J. Dupays, E. Daniel and N. Lupoglazoff, 2D Navier-StokesStability Computations for Solid Rocket Motors: Rotational, Combustion and Two-Phase Flow Effects, *AIAA, Vol. 3326*, 1997, 1-11.

[9] N. Lupoglazoff, and F. Vuillot, 2D NumericalSimulation of Vortex Shedding Phenomenon in 2D Test Case Solid Rocket Motors, *AIAA, Vol. 0776*, 1992, 1-9.

[10] K. Kirkkopru, D.R. Kassoy, Q. Zhao, UnsteadyVorticityGenerationandEvolution in a Model of a Solid Rocket Motor, *Journal of Propulsion and Power, Vol.12 (4)*, 1996, 646-654.

[11] P.L.Staab, Q. Zhao, D.R. Kassoy, K. Kirkkopru,AcousticallyGeneratedVorticity in an Internal Flow, *Journal of Fluid Mechanics, Vol. 413*, 2000, 247-285.

[12] P. Alavilli, J. Buckmaster, T. L. Jackson, and M. Short, Ignition-Transient Modeling for Solid Propellant Rocket Motors, *AIAA, Vol. 3567*, 2000, 1-9.

[13] S. Apte, and V. Yang, Unsteady Flow Evolution and Combustion Dynamics of Homogenous Solid Propellant in a Rocket Motor, *Combustion and Flame, Vol. 131 (1-2)*, 2000, 110-131.

[14] W. A. El-Askary, S. A. Wilson, and A. Hegab,Simulation of Reactive Fluid Flow in a Solid Rocket Motor Combustion-Chamber with/without Nozzle, *CMES, Vol. 76 (4)*, 2011, 235-266.

[15] W. W. Chu, V. Yang, J. Majdalani, PremixedFlameResponse to Acoustic Waves in a Porous-Walled Chamber with Surface Mass Injection, *Combustion and Flame, Vol. 133*, 2003, 359-370.

[16] M. Yumusak, *Non-ReactingandReacting Flow Analysis in Propulsion Systems*, Ph.D. Dissertation, Middle East Technical University at Ankara, 2000.

[17] G. P. Sutton, *Rocket Propulsion Elements*Wiley, New York, Ch. 11, 1992, pp. 417-437.

[18] M. Uygun, K. Kirkkopru, NumericalSimulation of Unsteady Flows in Solid Rocket Motors with Dual Time Stepping, *ITU Dergisi/d: Muhendislik, Vol. 8(2)*, 2009, 41-52.

[19] J. Terzic, B. Zecevic, S. Serdarevic-Kadic, and A. Catovic, 2012, NumericalSimulation of Internal Ballistics Parameters of Solid Propellant Rocket Motors, *15th Seminar "New Trends in Research of Energetic Materials"*, University of Pardubice, Part II, 881-892, ISBN 978-89-7395-480-2.

[20] Q. Li, G. He, P. Liu, and J. Li, Coupled Simulation of Fluid Flow and Propellant Burning Surface Regression in a Solid Rocket Motor, *Computers and Fluids, Vol. 93*, 2014, 146-152.

[21] D. Greatrix, Numerical Evaluation of the Use of Aluminum Particles for Enhancing Solid Rocket Motor Combustion Stability, *Energies, Vol. 8*, 2015, 1195-1215.

[22] J. Montesano, K. Behdinan, D.R.Greatrix, Z. Fawaz, InternalChamberModeling of a Solid Rocket Motor: Effects of coupled structural and acoustic oscillations on combustion, *Journal of Sound and Vibration, Vol. 311*, 2008, 20-38.

[23] L. Wang, Z. Wu, H. Chi, C. Lui, H. Tao, Q.Wang, NumericalandExperimental Study on the Solid-Fuel Scramjet Combustor, *Journal of Propulsion and Power, Vol. 31, No.2*, 2015, 685-693.

[24] M. J. Ward, S. F. Son, and M. Q. Brewster, Role of Gas- and Condensed-Phase Kinetics in Burning Rate Control of Energetic Solids, *Combustion Theory and Modeling, Vol. 2 (3)*, 1998, 293–312.

[25] R.D. Geckler, *SelectedCombustionProblems*AGARD, PermagonPress, New York, 1993.

[26] G. Gupta, L. Jawale, Mehilal, B. Bhattacharya, Various Methods for the Determination of the Burning Rates of Solid Propellants-An Overwiew, *Central EuropeanJournal of Energetic Materials, Vol.12(3)*, 2015, 593-620

[27] M. O. Havlucu, K. Kirkkopru, NumericalSimulation of Flow in a Solid Rocket Motor: Combustion Coupled with Regressive Boundary, *Journal of Multidisciplinary Engineering Science and Technology, Vol. 3 (1)*, 2016, 3790-3798.

[28] R. C.,Rogersand W.,Chinitz, Using a Global Hydrogen-Air Combustion Model in Turbulent Reacting Flow Calculations, *AIAA Journal, Vol 21. No.4*, 1982, 586-592.

[29] ANSYS/Fluent, Software Package, Ver. 15.0, ANSYS, Canonsburg, PA, 2013.

[30] P. Kuentzmann, Introductionto Solid Rocket Propulsion, Internal Aerodynamics inSolid Rocket Propulsion, *RTO Educational Notes EN-023*, 2004.

[31] B. Gossant, Solid PropellantCombustion and Internal Ballistics of Motors, *Solid RocketPropulsionTechnology*, PergamonPress, Oxford, 1993, pp. 111-191.

[32] Microsoft Visual C++ 2010 Express, Software Package, Ver. 10.0.30319.1, 2010.